The ratio of the carbon-containing gas components to the Si vapor are given from Eq. 8

$$\log(I_{SiC_2}/I_{Si}) = 17.19 - 4.47 \times \frac{10^4}{T}$$

$$\log(I_{Si_2C}/I_{Si}) = 2.96 - 1.02 \times \frac{10^4}{T}$$

The value of SiC_2 to Si ratio with increasing temperature is much above the values reported by Lilov.[7,8] This is due to the higher heat of sublimation from Si and SiC_2. The ratio of Si_2C to Si in the SiC–Si system is in good agreement with the values given by Lilov.

Conclusions

We studied the composition of the gas phase of SiC during sublimation by using a Knudsen cell and a quadrupole mass spectrometer in the temperature range 1900–2190°C. The heat of sublimation for Si, SiC_2, and Si_2C and their ratio of intensity to the Si component were determined. The variation of the SiC source material in grain size and polytype showed no significant difference for the heat of sublimation and the ratio of the vapor components, as expected. By addition of elemental silicon to the SiC powder at a weight ratio of 1/20, Si in the gas phase was dominated by the vaporization of elemental silicon. Our value of the heat of sublimation of the SiC_2 compound molecule in the SiC–C or SiC–Si system is much higher than in former publications.

Manuscript submitted December 1, 1997; revised manuscript received May 15, 1998.

The University of Erlangen-Nürnberg assisted in meeting the publication costs of this article.

REFERENCES

1. M. Ruff, H. Mitlehner, and R. Helbig, *IEEE Trans. Electron Devices*, **ED-41**, 1040 (1994).
2. M. Bhatnager and B. J. Baliga, *IEEE Trans. Electron Devices*, **ED-40**, 645 (1993).
3. R. I. Scace and G. A. Slack, in *Silicon Carbide-A High Temperature Semiconductor*, J. R. O'Connor and J. Smiltens, Editors, p. 24, Pergamon Press, Oxford (1960).
4. R. C. Glass, D. Henshall, V. F. Tsvetkov, and C. H. Carter, Jr., *Phys. Status Solidi B*, **202**, 149 (1997).
5. J. Drowart, G. De Maria, and M. G. Ingrahm, *J. Chem. Phys.*, **29**, 1015 (1958).
6. J. Drowart and G. De Maria, in *Silicon Carbide-A High Temperature Semiconductor*, J. R. O'Connor and J. Smiltens, Editors, p. 16, Pergamon Press, Oxford (1960).
7. S. K. Lilov, *Cryst. Res. Technol.*, **28**, 503 (1993).
8. S. K. Lilov, *Diamond Relat. Mater.*, **4**, 1331 (1995).
9. R. E. Honig, *J. Chem. Phys.*, **22**, 126 (1954).
10. D. Hofmann, Yu. N. Karpov, Yu. N. Makarov, E. N. Mokhov, M. G. Ramm, M. S. Ramm, A. D. Roenkov, and Yu. A. Vodakov, *Inst. Phys. Conf. Ser.*, **142**, 29 (1995).
11. Yu. A. Vodakov, E. N. Mokhov, M. G. Ramm, and A. D. Roenkov, *Krist. Tech.*, **14**, 729 (1979).
12. R. E. Honig, *J. Chem. Phys.*, **22**, 1610 (1954).

Highly Purified Silane Gas for Advanced Silicon Semiconductor Devices

Atsushi Ohki,[a] Tadahiro Ohmi,*[a] Junichi Date,[b] and Takahiko Kijima[b]

[a]*Department of Electronic Engineering, Graduate School of Engineering, Tohoku University, Aoba, Sendai 980-77, Japan*
[b]*Osaka Sanso Kogyo Limited, Saitama 355, Japan*

ABSTRACT

Highly purified SiH_4 gas is required for manufacturing silicon semiconductor devices (e.g., the formation of Si-single crystal, poly-Si, Si_3N_4, and siliside thin films. We have newly established a technology for delicately measuring impurities in SiH_4 gas by using a modified atmospheric pressure ionization mass spectrometer equipped with a two-compartment ion source, with a lower detection limit around 0.1 to 1 ppb. We have succeeded in establishing the quantitative analysis method for disiloxane in SiH_4 gas by developing a new technology for generating a Si_2H_6O standard gas. This is a perfect reaction between H_2O and SiH_4 in the reactor. Its lower detection limit is 1 ppb. This analysis technology clarified that SiH_4 and H_2O changed rapidly into molecules containing oxygen atoms in the cylinder or supply tubing system (i.e., disiloxane, trisiloxane, ... and particles). Therefore, this result shows that the impurities in SiH_4 gas to be controlled are not H_2O but siloxane and particles. Based on this technology, we have completed development of technology for manufacturing high purity SiH_4 gas free from H_2O, siloxane, and particles. In addition, we have established a technology for delivering highly purified SiH_4 gas to the point of use. It is expected that enhanced wafer yield and higher quality thin film will be ensured in the silicon semiconductor device manufacturing process.

Introduction

Along with further integration of semiconductor devices, there has been an increasing need for higher quality thin film and enhanced yield.[1,2] So far, clean process-chambers without outgases, particle and metal contamination; high speed pumping system for discharging reaction products from the chamber, and an ultraclean gas distribution system have been developed.[3-7] Therefore, it has been clear that the semiconductor process is influenced by the quality of special gases which are used directly for thin film formation.

The main gas used for thin film formation (Epi-Si, poly-Si, Si_3N_4, and silicides growth film) is SiH_4 in the semiconductor device manufacturing process. A key impurity in SiH_4 gas is a H_2O molecule. It is believed that the mixing of H_2O into SiH_4 would generate particles in the chamber or oxides in thin films to be formed, thereby decreasing yields or causing deterioration of thin film quality.

The conventional atmospheric pressure ionization mass spectrometer (APIMS) is able to detect impurities in noncorrosive gas and in nondeposition gas such as N_2 gas, Ar gas, and H_2 gas, in part per trillion (ppt) order.[8,9] However, a measurement technology for ensuring a detection sensitivity of a ppt has not yet been developed with regard to impurities in specialty gas having reactive and corrosive characteristics. At present, gas chromatography (TCD, FID, PID, DID, MS, etc.), moisture meter (crystal-oscillation type, electrolysis type etc.), optical measurements (infrared ray absorption, laser ray absorption, etc.) are used to measure impurities in specialty gas.[10-16] The detection limit of these conventional methods, however, is limited to 10–100 ppb, and they cannot be applied to highly sophisticated impurity measurement at 1 ppb or less which will be needed in the future. A measurement technology

* Electrochemical Society Active Member.

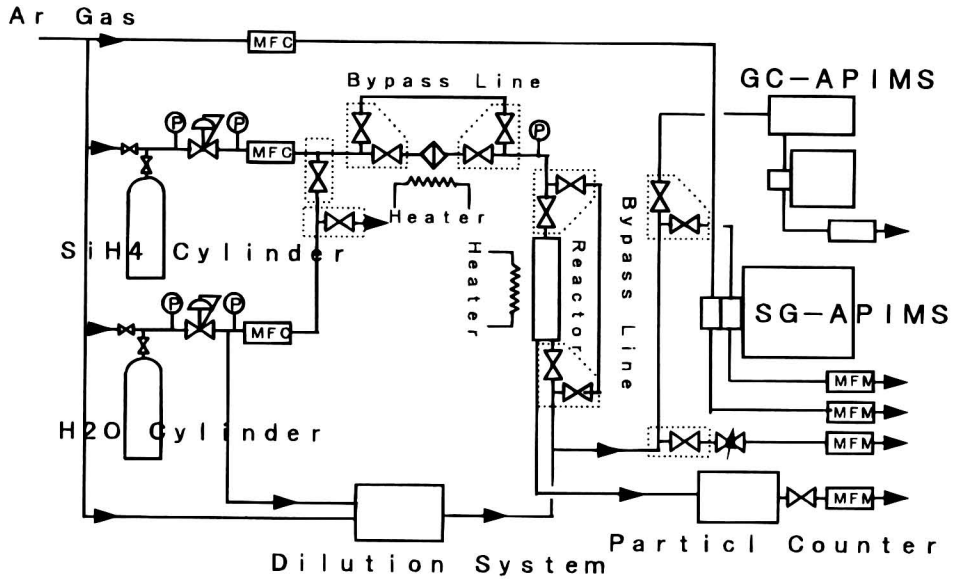

Fig. 1. Schematic flow diagram of the experimental system.

with a detection limit of 1 ppb or less is currently under development to measure impurities in specialty gas.[17]

We have developed a sophisticated technology to detect impurities in SiH_4 gas at 1 ppb or less.[18] This new technology could not be developed without the modified APIMS which was developed by Hitachi Tokyo Electronics Co. Ltd. and us. The conventional APIMS can measure impurities with a sensitivity in the order of ppt but it cannot be used for corrosive and deposition gas. The modified APIMS equipped with a two-compartment ion source can measure impurities in both corrosive gas and in deposition gas due to a stable ionization reaction. In addition, we have succeeded in establishing a quantitative analysis method for disiloxane in SiH_4 gas. The standard gas has not been produced because such technology was not available.

Based on this measurement technology, we have found that H_2O mixed into SiH_4 turns to disiloxane, polymer siloxane, and particles, and we have developed a high-purity SiH_4 gas (siloxane concentration is less than 1 ppb) delivery system.[19,20]

It is expected that using this technology will bring about enhanced wafer yield and higher quality thin film in the silicon semiconductor manufacturing process.

Experimental

Figure 1 shows the experimental flow. The experimental system is equipped with such measurement tools as GC-APIMS, SG-APIMS, and particle counters. GC-APIMS is high-sensitivity mass spectroscopy which separates and extracts gaseous impurities by means of gas chromatography, ionizes the extracted impurities at atmospheric pressure, and detects them. Its detection sensitivity is in the order of ppt. Figure 2 shows a flow chart to describe gas chromatography. It employs an integrated diaphragm valve. The flow rate is precisely controlled with a mass-flow controller (MFC). The diameter of the gas tube is 1/16 of an inch.

SG-APIMS is equipped with two atmospheric ionization compartments as shown in Fig. 3. Ar gas and SiH_4 gas are introduced to the first and second ionization compartments, respectively. An Ar^+ ion generated by means of a corona discharge in the first ionization compartment is sent out to the second ionization compartment. In the second compartment, Ar^+ ion reacts with an impurity in the specialty gas to exchange ion, and consequently, impurity ions are generated in the specialty gas in large amounts. Due to this mechanism, SG-APIMS features high sensitiv-

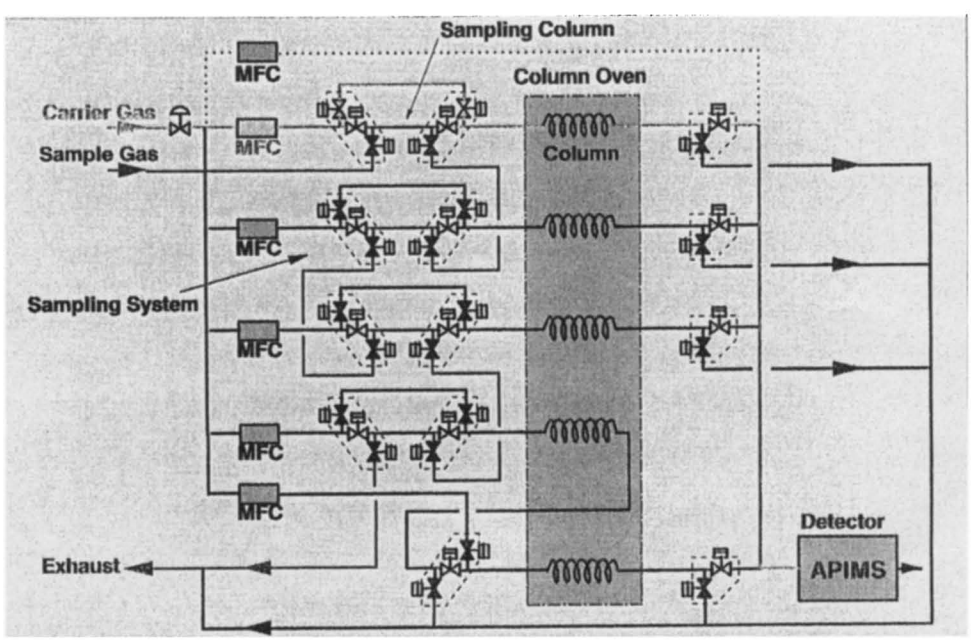

Fig. 2. Schematic flow diagram of the gas chromatography used (GC-APIMS).

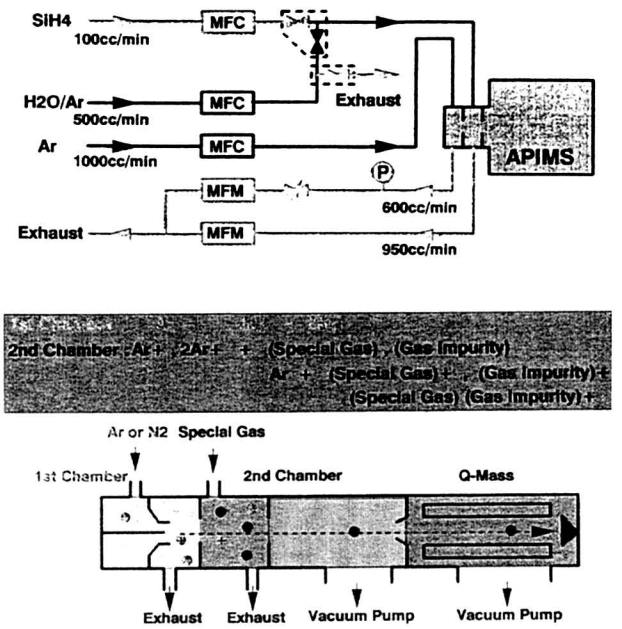

Fig. 3. Schematic diagram of SG-APIMS.

ity of ppt to ppb. SG-APIMS was developed by Hitachi Tokyo Electronics, Ltd., and us.

The particle measurement system employs a laser-type particle counter KC90 manufactured by Rion Co.,Ltd. Gas sampling is set at a flow of 10 cm^3/min.

The following experiments were conducted by using the experiment system shown in Fig. 1. First, in order to verify the possibility of measuring H_2O in SiH_4 gas, H_2O injected to SiH_4 gas was measured with SG-APIMS. The concentration of H_2O injected was varied from 1 to 200 ppb to prepare the calibration curve of H_2O in SiH_4 gas. H_2O was injected right before APIMS inlet. It was controlled below 5 s from when H_2O was injected to SiH_4 gas to when SiH_4 gas was introduced to SG-APIMS. SiH_4 (100 cm^3) was taken as a sample every minute.

In the second experiment, in order to verify quality of SiH_4 gas, three SiH_4 gases available in the market were compared each other in terms of H_2O concentration with SG-APIMS. These three gases were manufactured in a different way.

Further H_2O behavior was studied while H_2O was injected to SiH_4 gas cylinder. H_2O of 0.1, 1, and 10 ppm was injected to each of three SiH_4 gas cylinders, and H_2O behavior was evaluated with SG-APIMS and GC-APIMS. Pressure in these gas cylinders was controlled at 3 MPa, and was measured 7 days and 1 year after they were filled with gas. These Al cylinders, filled with SiH_4 gas to a capacity of 10 L were preliminarily treated in the following way

(*i*) H_2O/Ar gas of $(0.6\ MPa)_{absolute}$ was placed in the cylinders which had been pumped down. (H_2O/Ar gas concentration was varied to 0.25, 2.5, and 25 ppm.)

(*ii*) SiH_4 gas was filled to $(2.4\ MPa)_{absolute}$.

For the measurement with GC-APIMS, N_2 (35 cm^3/min) was introduced as a carrier gas, and a column of 30% DC200 on chromsorb P (6m, 60/80 mesh, 60°C) was used.

In the third experiment, SiH_4 gas was exposed to metal filter to study behavior of siloxane and H_2O. A metal filter features the largest surface area among components mounted onto a gas delivery system. Ni filters and stainless steel filters (SUS316L) were tested. They were purged with inert gas at room temperature or at 400°C before being used in the experiment. Also, H_2O of 0.5 to 10 ppm was injected to SiH_4 gas upstream of the filter. The flow rate of SiH_4 gas to be delivered to the filter was controlled at 50 cm^3/min. All of the SiH_4 gas passing through the filter was introduced to SG-APIMS.

The fourth experiment was conducted to evaluate the rate of disiloxane generation induced by H_2O-SiH_4 reaction. SiH_4 gas and H_2O were mixed in a reactor to obtain the amount of H_2O and disiloxane as a function of reaction time (retention time in reaction tube). The reactor (SUS316L) featured a capacity of 350 cm^3 and surface area of 385 cm^2. Reaction time was controlled by varying the SiH_4 gas flow rate. SG-APIMS was employed as a measurement tool. Particle count was also evaluated in SiH_4 gas coming out from the reactor tube to obtain the relationship among H_2O, disiloxane, and particles.

Moreover, in order to obtain the calibration curve concerning disiloxane, SiH_4 gas and H_2O gas was made to react completely in the reactor to produce disiloxane gas and H_2 gas. Formula 1 indicates that the H_2O volume introduced in the reactor and generated disiloxane volume are in the proportion of one to one

$$2SiH_4 + H_2O \rightarrow SiH_3\text{-}O\text{-}SiH_3 + 2H_2 \qquad [1]$$

Therefore, additional H_2O was regarded as disiloxane concentration and a disiloxane calibration curve was obtained from the relationship between additional H_2O volume and disiloxane ion intensity. The conditions of that reaction are as follows; H_2O and disiloxane adsorbed on the reactor surface were removed by baking the reactor at 150°C with a supply of SiH_4 gas. After that, the reactor was cooled at 22°C and made H_2O supplied to the reactor, adsorb on the surface by introducing H_2O/Ar gas at 50 cm^3/min for 10 min. The H_2O concentration in the introduced Ar gas is 0.5, 1, 2, 3, and 5 ppm. Moreover, we supplied the reactor with SiH_4 gas at 50 cm^3/min and measured total disiloxane volume discharged from the reactor. The reactor was heated from 22 to 150°C for 15 min in order to discharge disiloxane completely and quickly.

Last, highly purified SiH_4 cylinder gas was produced and impurities in this gas were measured. The purification technology for this SiH_4 gas used was a distillation method. The

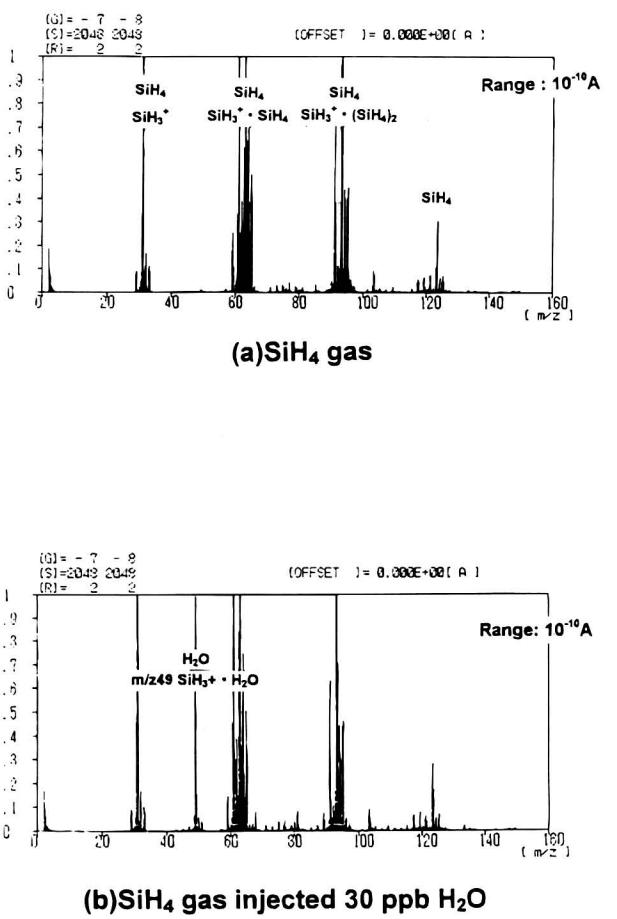

Fig. 4. SiH_4 gas spectra by SG-APIMS. (a) SiH_4 gas and (b) SiH_4 gas injected 30 ppb H_2O.

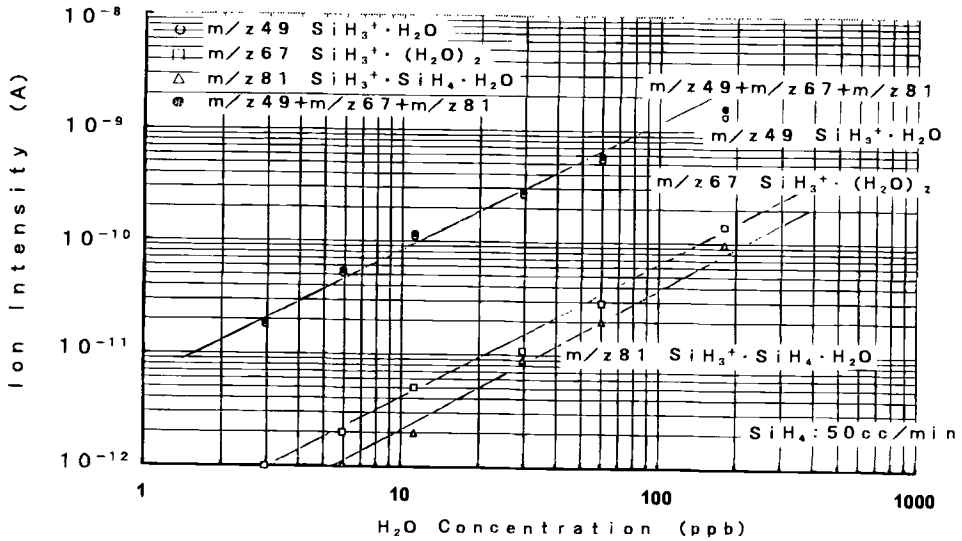

Fig. 5. H_2O calibration curve in SiH_4 gas.

SiH_4 distillation system and filling system made use of a stainless steel tube with a Cr_2O_3 surface treatment. The cylinder for high-purity SiH_4 gas used the clean stainless steel cylinder (without adsorbed H_2O) which resists heat up to 200°C by equipping the cylinder valve with a mounting-removing soluble plug. The purification system, the filling system, and the cylinder were purged out sufficiently by SiH_4 gas to remove adsorbed H_2O perfectly (in order to remove H_2O easily by changing H_2O to Si_2H_6O).

Results and Discussion

Figures 4a and b show spectra of SiH_4 gas obtained by SG-APIMS measurement. Figure 4a shows a spectrum of SiH_4 gas from a cylinder while Fig. 4b shows a spectrum of SiH_4 gas to which H_2O of 30 ppb is injected before SG-APIMS. The vertical axis corresponds to ion intensity, while the horizontal axis shows mass number. When comparing Fig. 4a and b, it is found that ion intensity of peaks with mass numbers of 49, 67, and 81 gets higher in the spectrum of SiH_4 gas with H_2O injected, which demonstrates that these are H_2O-related peaks.

Figure 5 shows a calibration curve of H_2O in SiH_4 gas obtained by varying concentration of H_2O injected to SiH_4 gas. The horizontal axis shows the amount of H_2O added to SiH_4 gas (H_2O concentration in SiH_4 gas) while the vertical axis shows the ion intensity of peaks with mass numbers of 49, 67, and 81, and total ion intensity of these three peaks. H_2O concentration is found proportional to total ion intensity of the three peaks when H_2O in SiH_4 gas is in the range of 1-200 ppb.

We conclude the following based on these results. In the spectrum shown in Fig. 4, ion intensity of SiH_3^+ is the highest. Ionization energy of SiH_4 and H_2O is almost the same, 12.8 and 12.6 eV, respectively. Therefore, SiH_4, which is a major component, gets ionized mainly to generate SiH_3^+ ion (m/z 31).[2] The H_2O-related ion is considered to be generated when SiH_3^+ ion and H_2O molecule are clustered. Peaks with mass numbers of 49, 67, and 81, which increase when H_2O is injected to SiH_4 gas, are cluster ions containing H_2O. If it can be assumed that they correspond to SiH_3^+ H_2O SiH_3^+ $(H_2O)_2$, and SiH_3^+ SiH_4 H_2O, respectively, the experimental results are reasonably explained. The ion intensity of the peak with mass number 64 is the highest, and it is another clustered SiH_4 (SiH_3^+, SiH_4) just like that of mass number 31.

Figure 6a, b, and c show SG-APIMS the spectra of three types of SiH_4 gas with manufactured in a different way. No peaks of H_2O (m/z 49, 67, and 81) are detected in any SiH_4 gas cylinders. According to the calibration curve shown in Fig. 5, the H_2O concentration in SiH_4 cylinders sold on the market is found below 1 ppb.

Figures 7 shows the SG-APIMS spectrum of SiH_4 gas contained in the cylinder to which H_2O is injected. Spectrum 7a represents SiH_4 gas to which no H_2O is injected. Spectra 7b, c, and d represent SiH_4 gas with H_2O of 0.1, 1, and 10 ppm, respectively. Pressure for filling a cylinder is 3 MPa, and mixing ratio of gases in cylinder is 80% SiH_4, 20% Ar gas, and H_2O. Figures 7b and b′, c, and c′, and d

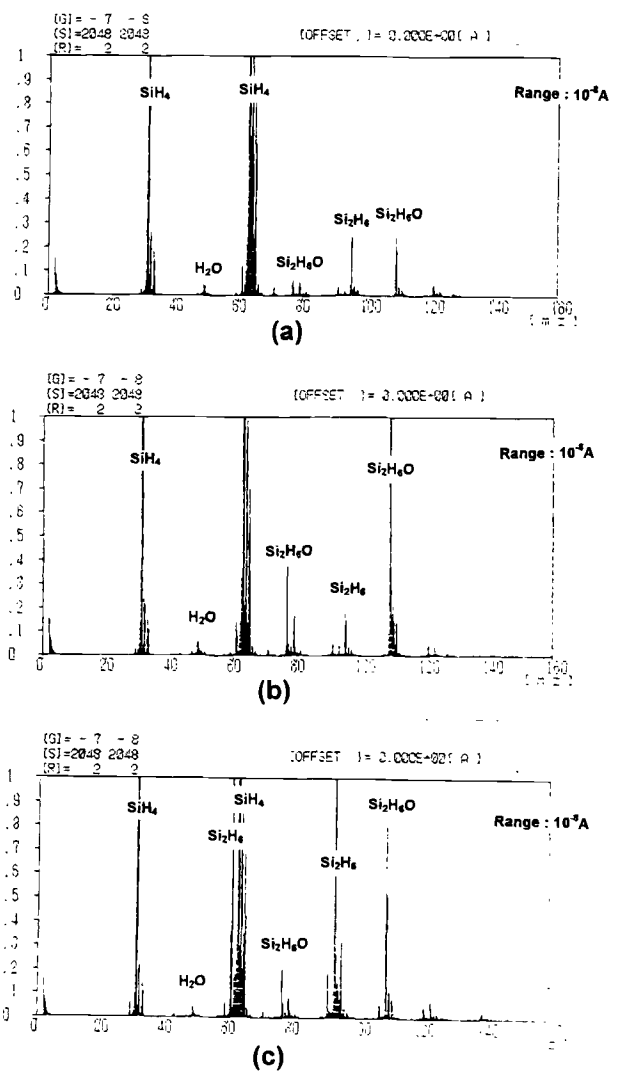

Fig. 6. SiH_4 gas spectrum of three types of cylinders.

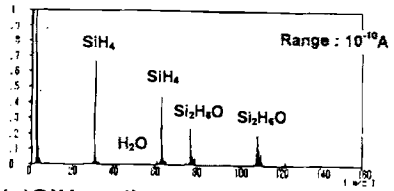

(a)SiH_4 cylinder injected no H_2O

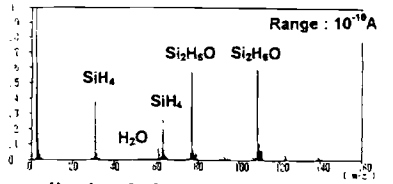

(b)SiH_4 cylinder injected 0.1 ppm H_2O (7 days)

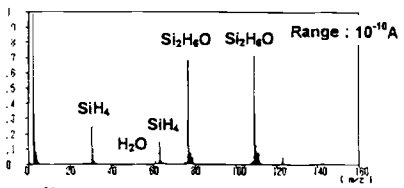

(c)SiH_4 cylinder injected 1 ppm H_2O (7 days)

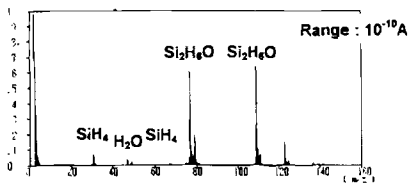

(d)SiH_4 cylinder injected 10 ppm H_2O (7 days)

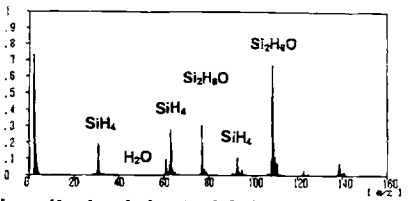

(b')SiH_4 cylinder injected 0.1 ppm H_2O (1 year)

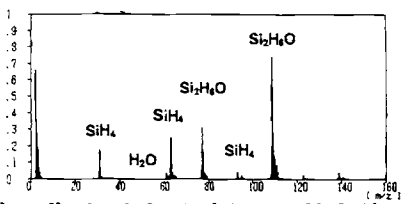

(c')SiH_4 cylinder injected 1 ppm H_2O (1 year)

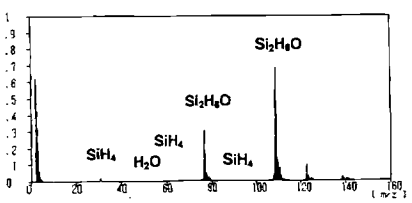

(d')SiH_4 cylinder injected 10 ppm H_2O (1 year)

Fig. 7. SiH_4 gas spectra of SiH_4 cylinder injected H_2O (7 days and 1 year). (a) SiH_4 cylinder injected, no H_2O. (b) 0.1 ppm H_2O (7 days). (c) 1 ppm H_2O (7 days). (d) 10 ppm H_2O (7 days). (b') 0.1 ppm H_2O (1 year). (c') 1 ppm H_2O (1 year). (d') 10 ppm H_2O (1 year).

and d' are spectra from the same cylinders, respectively. Figures 7b, c, and d show SG-APIMS spectra of SiH_4 gas with an elapsed time of 7 days after filling, and 7b', c', and d' show SG-APIMS spectra of SiH_4 gas with an elapsed time of 1 year after filling.

In Fig. 7a, b, and c, none of H_2O-relevant peaks, with mass numbers of 49, 67, or 81, are detected, although SiH_4 gas with H_2O injected is evaluated. Ion intensity of SiH_4-relevant peaks with m/z 31 (SiH_3^+) and 63 ($SiH_3^+ \cdot SiH_4$) gets lower. Ion intensity of peaks with mass numbers of 77 and 109 gets higher due to H_2O injection. The peaks with mass numbers of 77 and 109 are found to be the most intense. In order that measurement results of Fig. 7b, c, d, and 7b', c', d' are comparable; the filled cylinders stood for 7 days, after which the quantity of disiloxane in SiH_4 gas is unchanged.

Peaks with mass numbers of 77 and 109 are not relevant either to H_2O or stable compounds which may be formed through combination of Si and H elements.

Figure 8 shows a GC-APIMS chromatogram taken from the same four SiH_4 gas cylinders as those shown in Fig. 7. The column is composed of 30% DC200 on chromsorb P (5m, 50/80 mesh, 60°C). The flow rate of carrier gas is set at 35 cm^3/min. In Fig. 8, where H_2O is added to SiH_4 gas, a peak with mass number of 77 is detected when retention time is 8 min. Retention time of this peak is twice as long as that of SiH_4 peak. Ion intensity of SiH_4 gas with 0.1, 1, and 10 ppm H_2O added is 8.5×10^{-11} A, 2.9×10^{-10} A, and 8.8×10^{-10} A, respectively. The ion intensities of peaks found to be proportional to H_2O concentration. Even in the SiH_4 gas cylinder with no H_2O added, a peak with mass number of 77 is detected, although it is very low in ion intensity: 1.2×10^{-11} A. The SEMI Standard describes that disiloxane, methyl siloxane, and the like can be detected under the measurement conditions used in the experiment shown in Fig. 8.

Based on the experimental results shown in Fig. 7 and 8, it can be concluded that peaks with mass numbers of 77 and 109 stand for disiloxane (SiH_3-O-SiH_2^+) and clusters of disiloxane and silane molecules (SiH_3-O-SiH_2^+ SiH_4), and disiloxane (SiH_3-O-SiH_3) is generated due to H_2O injection. As the ionization energy of disiloxane is lower than that of SiH_4, the disiloxane molecule is more likely to be ionized than the SiH_4 molecule. This is why disiloxane is detected with high sensitivity. If siloxane whose ionization energy is low exists in more than several hundreds parts per billion, the SiH_4 ion with high ionization energy can be reduced, which provides a good explanation for the result shown in Fig. 7.

Based on these findings, the H_2O mixed into a SiH_4 gas cylinder cannot exist as a H_2O molecule, but reacts instead with SiH_4 to generate disiloxane. As a result, the impurity which we must measure is disiloxane in SiH_4 gas.

Figure 9 shows the behavior of H_2O, disiloxane, and Si_2H_6 evaluated with SG-APIMS at an outlet of the metal filter to which SiH_4 gas is introduced. The filter shown in Fig. 9a uses a Ni media which is purged at room temperature. The filter shown in Fig. 9b uses a SUS316L media which is purged at room temperature. The filter shown in Fig. 9c uses a SUS316L media which is purged at 400°C. Purge conditions are as follows: (*i*) high-purity Ar gas (with H_2O concentration of 1 ppb or less), (*ii*) flow rate of 1 L/min, and (*iii*) purge time of 24 h. After the purge, the H_2O concentration measured at the filter outlet is found below 1 ppb in every filter.

Figure 9 shows ion intensity of each element on the vertical axis and the elapse of time from SiH_4 gas introduction in the filter on the horizontal axis. SiH_4 (m/z 63), H_2O

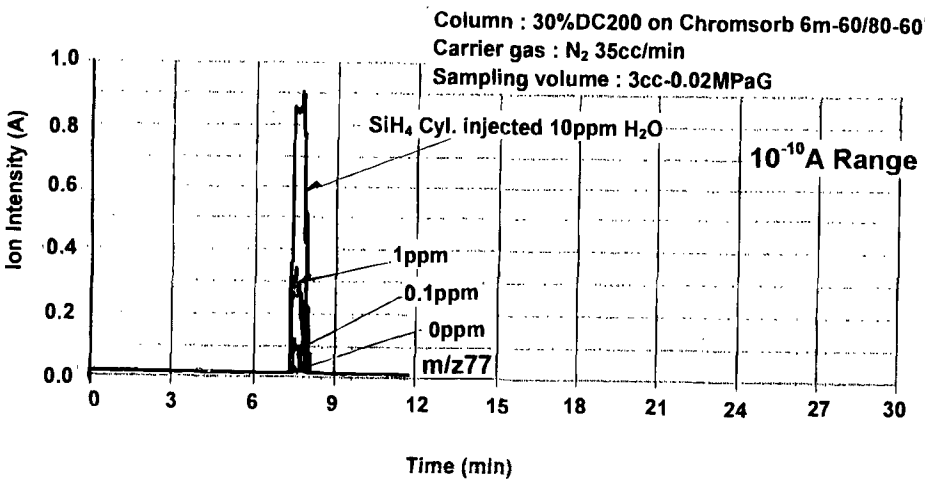

Fig. 8. SiH_4 gas chromatograms of SiH_4 cylinders injected H_2O (0, 0.1, 1, 10 ppm).

(m/z 49), siloxane (m/z 77), and Si_2H_6 (m/z 61) ions are monitored. It has been verified that Si_2H_6 is detected as $Si_2H_5^+$ (m/z 61) with SG-APIMS when it is injected to SiH_4 gas. As shown in Fig. 9, the concentration of H_2O (m/z 49) does not change due to SiH_4 gas introduction in any of the three filters (H_2O concentration: 1 ppb or less). Siloxane

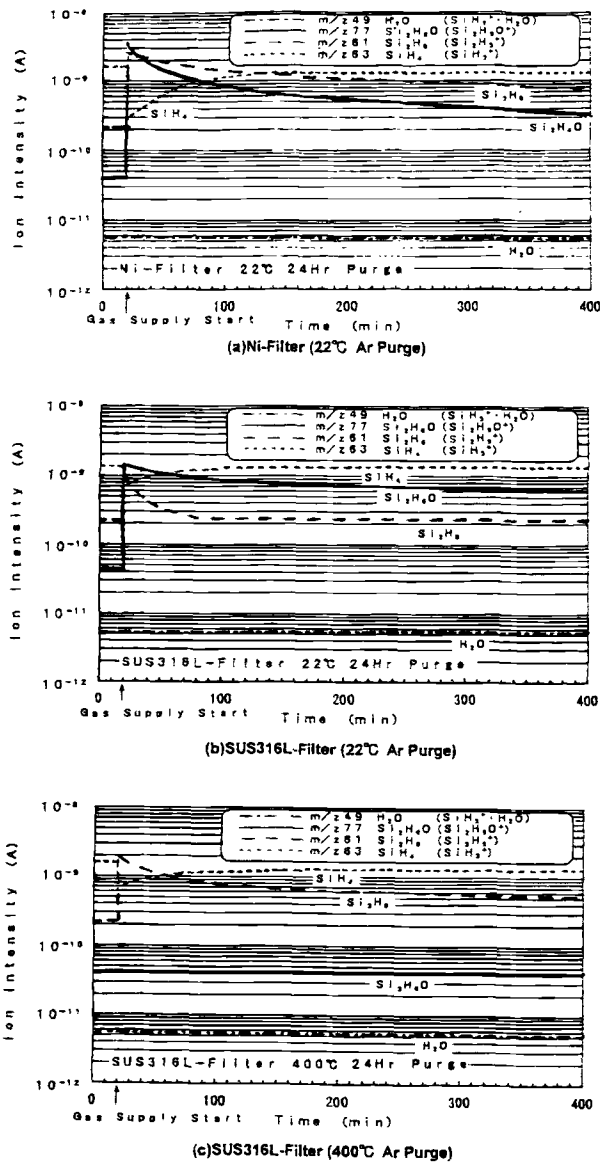

Fig. 9. Behavior of H_2O, Si_2H_6O, and Si_2H_6 in SiH_4 (metal filter).

concentration does not change in the case of the SUS316L filter baked at 400°C. In the case of two filters which are purged at room temperature (shown in a and b), the ion intensity of siloxane increases to over ten times as soon as SiH_4 gas is introduced, and then it gets lower gradually. This result indicates the following facts. When a filter is baked at 400°C for a purge, H_2O adsorbed on its surface is completely desorbed and removed. A purge at 25°C, however, does not completely remove H_2O from a filter surface, allowing H_2O to remain adsorbed.[19] When H_2O remains adsorbed on a filter surface, even if no H_2O gets released from filter media, SiH_4 introduced immediately reacts with H_2O adsorbed on the surface to generate siloxane. The generated siloxane mixes with SiH_4 gas to constitute an impurity containing an oxygen atom.

Si_2H_6 concentration gets higher by SiH_4 gas introduction in the following order of Ni filter < SUS316L filter (purged at 400°C) < SUS316L filter (purged at room temperature). It is known that a surface catalytic effect for SiH_4 gas decomposition is stronger in the order of Ni, SUS316L (purged at 400°C), and SUS316L (purged at room temperature).[20] The Si_2H_6 increase shown in Fig. 9, therefore, reflects a catalytic reaction of surface. SiH_4 is decomposed to generate Si_2H_6.

Figure 10 shows H_2O concentration as a function of siloxane concentration when SiH_4 gas containing H_2O is introduced to a SUS316L filter. H_2O is injected upstream of the filter. Concentration of H_2O injected is varied from 0.5 to 10 ppm. Flow rate of SiH_4 is controlled at 50 cm^3/min. Figure 10 indicates that H_2O of 10 ppm or less reacts with SiH_4 completely within 30 s (time for SiH_4 gas to go through filter). It is known that the component concentration is proportional to the ion intensity when the main peak exists sufficiently in the SG-APIMS evaluation. This means that the amount of generated siloxane is proportional to H_2O concentration.

Figure 11 shows a relationship between H_2O-SiH_4 coexisting time, siloxane generation, and residual H_2O. A reactor with a capacity of 350 cm^3 and surface area of 385 cm^2 is used in this evaluation. As shown in Fig. 11, as the reaction time gets longer, H_2O reduction and disiloxane increase are accelerated. The reaction between SiH_4 and H_2O to generate disiloxane is not completed in seconds but proceeds slowly.

Results shown in Fig. 10 and 11 seem to indicate two contradicting facts. For the case of the filter shown in Fig. 10, the reaction to generate siloxane features the reaction ratio within 30 s at 100%. For the case of the reaction tube shown in Fig. 11, however, the reaction ratio within 30 s is below 5%. The difference in these two experiments indicates that the reaction to generate siloxane mainly takes place on the stainless steel surface. The effective surface area of the filter is 0.7 m^2 while the surface area of the reactor is 0.04 m^2: the filter has 18 times as much surface area as the reactor. In other words, the reaction rate of siloxane generation is restricted by the retention time of SiH_4 on the surface.

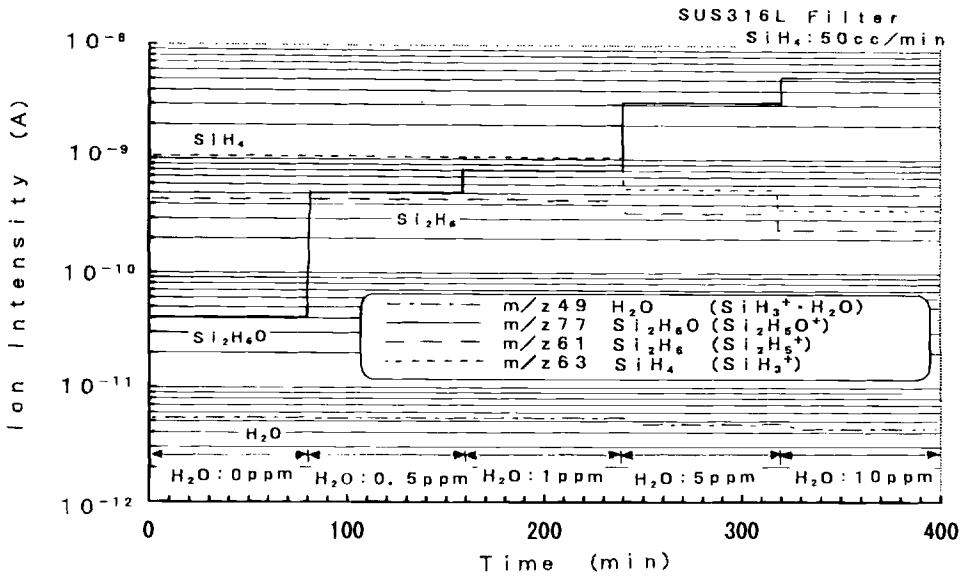

Fig. 10. The relationship between H_2O and Si_2H_6 in SiH_4 (SUS316L filter).

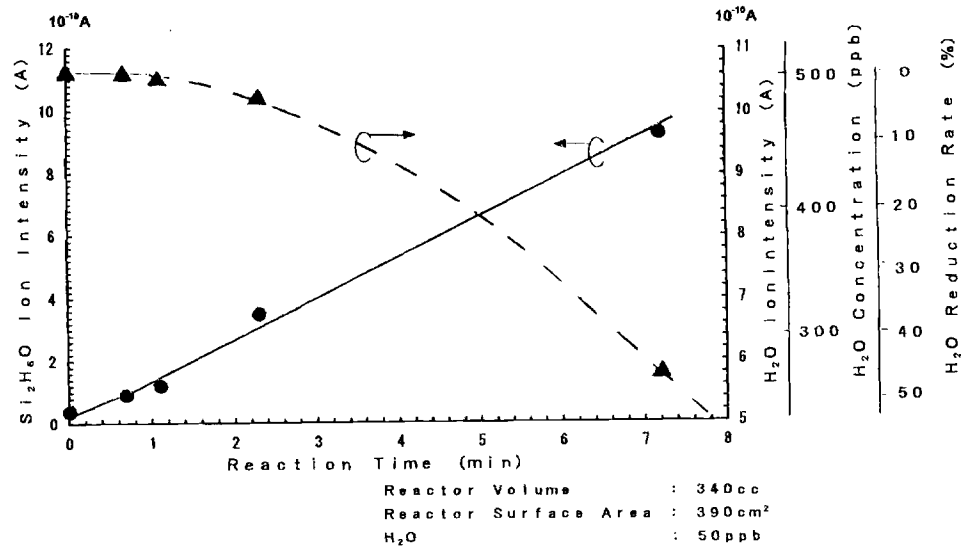

Fig. 11. The relationship between H_2O and Si_2H_6 in SiH_4 (reactor).

Figure 12 shows the number of particles generated when H_2O and SiH_4 coexist. SiH_4 gas with 0.5 to 10 ppm H_2O was supplied to the reactor for 1 h and enclosed for 5 h. Then, the enclosed SiH_4 gas was removed from the reactor and introduced to a particle counter by using SiH_4 without H_2O. As shown in Fig. 12, it was found that the amount of generated particles was proportional to the H_2O concentration.

The series of experiments have revealed that the coexistence of SiH_4 and H_2O induces the generation of gaseous disiloxane and solid particles at room temperature. It is not understandable, however, that what is generated is limited to disiloxane and particles. As is shown in Fig. 13, it is very likely that a polymer siloxane derivative, an intermediate, is simultaneously generated by the participation of H_2O.

By using a reaction that produces disiloxane in this study, a disiloxane calibration curve was obtained, in a range which was not previously obtained (indicated in Fig. 14). The horizontal axis shows H_2O volume absorbed on the reactor surface, and the vertical axis stands for total disiloxane ion intensity generated from SiH_4 gas and adsorbed H_2O. H_2O absorbed on the reactor surface was obtained by introduction of H_2O standard gas (Ar gas balance) into the reactor. It is obvious that total disiloxane ion intensity is proportional to absorbed H_2O. Also, for absorbed H_2O less than 5 mol, the curve is able to describe that disiloxane is singly generated because the detection intensity of silanol (m/z 47) and trisiloxane (m/z 123) are less than 5% for disiloxane ion intensity. Therefore, absorbed H_2O volume and generated total disiloxane volume are in a proportion of one to one. That is, the relationship between disiloxane concentration and disiloxane ion intensity is

$$C_{\text{disiloxane}} = 3.73 \times 10^{11} \times \text{I.I}$$

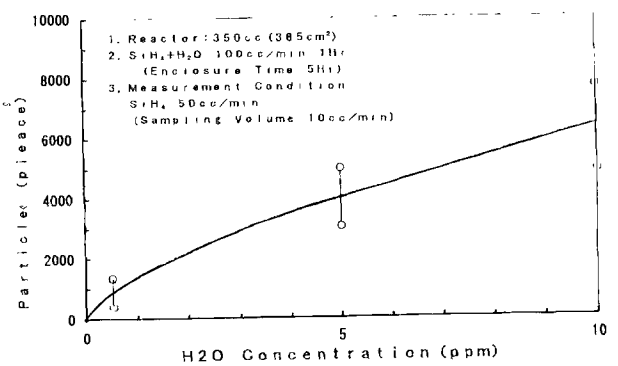

Fig. 12. The number of particles generated for various H_2O concentrations.

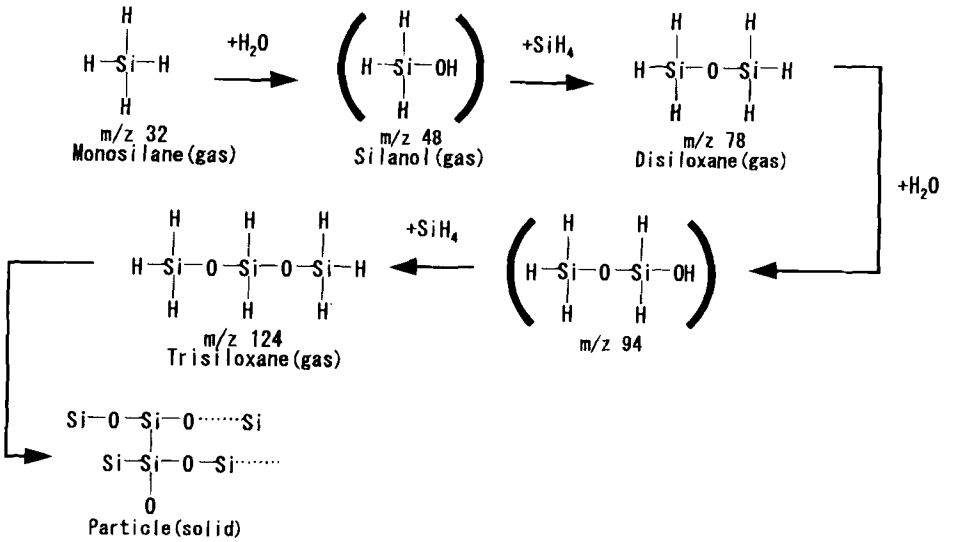

Fig. 13. Generation of siloxane and particles formed due to coexistence of SiH_4 and H_2O.

$$2SiH_4 + H_2O \rightarrow SiH_3\text{-}O\text{-}SiH_3 + 2H_2 \quad \cdots m/z77$$
$$(\ SiH_4 + H_2O \rightarrow SiH_3OH + H_2 \quad \cdots m/z47\ )$$
$$(\ SiH_4 + SiH_3OH \rightarrow SiH_3\text{-}O\text{-}SiH_3 + H_2\ )$$

$$SiH_4 + SiH_3\text{-}O\text{-}SiH_3 + H_2O \rightarrow SiH_3\text{-}O\text{-}SiH_2\text{-}O\text{-}SiH_3 + 2H_2 \quad \cdots m/z123$$
$$(\ SiH_3\text{-}O\text{-}SiH_3 + H_2O \rightarrow SiH_3\text{-}O\text{-}SiH_2\text{-}OH + H_2 \quad \cdots m/z94$$
$$SiH_3\text{-}O\text{-}SiH_2\text{-}OH + SiH_4 \rightarrow SiH_3\text{-}O\text{-}SiH_2\text{-}O\text{-}SiH_3 + H_2\ )$$

$C_{disiloxane}$: disiloxane concentration (ppb)

$I.I_{disiloxane}$: disiloxane ion intensity (A)

In these experimental conditions, generated trisiloxane volume increases greatly by reason of the further reaction of generated disiloxane and already absorbed H_2O, as absorbed H_2O is more than 5 mol. And also, the generated volume of silanol, which is an intermediate product from the reaction of disiloxane production, increases. As absorbed H_2O is less than 5 mol, the ratio of generated disiloxane volume is low, because absorbed H_2O is consumed by generation of silanol and trisiloxane.

At last, a highly purified SiH_4 gas, filled in cylinder, was produced using this study. Figures 15a and b show SG-APIMS spectra of this highly purified SiH_4 gas and conventional SiH_4 gas in the cylinder. The high purified SiH_4 gas is produced by the distillation method (boiling point The SiH_4, 112°C, Si_2H_6O, −15°C). Figure 16 shows the distillation system for the high purity SiH_4 gas production. The SiH_4 distillation system and filling system were made of stainless steel tubing with a Cr_2O_3 passivation surface which has characteristics of rapid H_2O desorption, little absorbed moisture volume, and noncabalistic effect.

The cylinder for high purity SiH_4 gas was a clean stainless steel cylinder which resists heat to 200°C by equipping the cylinder valve with a mounting-removing soluble plug in order to desorb H_2O adsorbed in the cylinder. The purification system, the filling system, and the cylinder were purged sufficiently with SiH_4 gas to remove adsorbed H_2O perfectly (by changing H_2O to Si_2H_6O). The filling pressure for the highly purified SiH_4 in the cylinder is $(4\ MPa)_{gauge}$. In the spectrum shown in Fig. 15, it is understood that Si_2H_6O concentration and H_2O concentration of the high purity SiH_4 gas are 5 ppb and less than 1 ppb, respectively.

Conclusion

By using SG-APIMS, we have established a new technology which allows for measurement of impurities (H_2O,

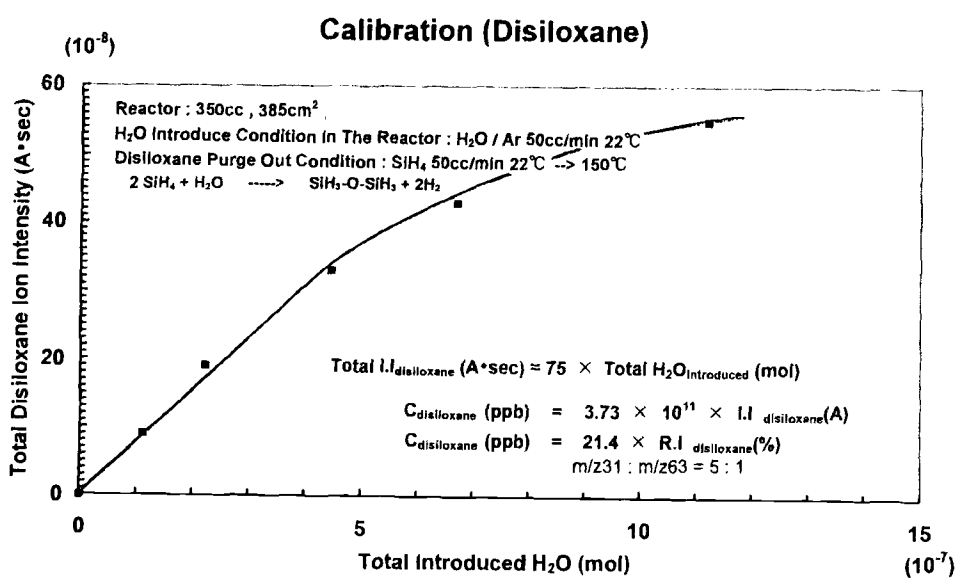

Fig. 14. The disiloxane calibration curve by using reaction SiH_4 and H_2O.

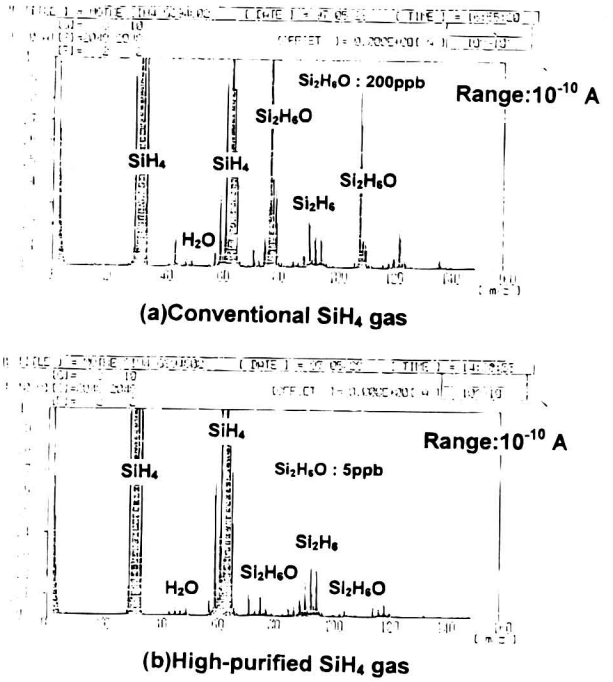

Fig. 15. The SG-APIMS spectra of SiH_4 gas in the cylinder.

siloxane, Si_2H_6, etc.) in SiH_4 gas at parts per thousand to parts per billion levels. In addition, we have succeeded in establishing the quantitative analysis method of Si_2H_6O in SiH_4 gas was established. This new measurement technology was used to confirm the following.

H_2O (H_2O adsorbed on a surface as well as gaseous H_2O in SiH_4 gas) reacts with SiH_4 in a cylinder and a gas distribution system to generate siloxane, siloxane derivatives, and particles. H_2O does not coexist with SiH_4. Generation of siloxane and particles is mostly induced by a surface reaction. In components featuring a large effective surface area such as a filter, this reaction finishes quickly, in around several tens of seconds.

The past quality control of SiH_4 cylinder focused on H_2O as an impurity in gas containing oxygen atoms. This study has revealed that it is not H_2O but siloxane, toward which attention should be directed as an impurity with oxygen atoms when using SiH_4 gas.

In addition, Ni and stainless steel baked at 400°C, feature a strong catalytic activity which accelerates self-decomposition of SiH_4.

These findings tell us that the following requirements must be satisfied in a high-purity SiH_4 gas distribution technology for the advanced device manufacturing process

1. Siloxane and particles must be controlled in SiH_4 gas to be delivered.
2. H_2O adsorbed onto a gas delivery system must be reduced to an ultimate level.
3. Processes and systems where H_2O are mixed must be minimized (by displacing with inert gas, with external leakage, etc.).
4. Gas delivery systems must use materials having a low catalytic activity which accelerates self-decomposition of SiH_4.

We have developed a cylinder for high purity SiH_4 gas (concentrations of Si_2H_6O and H_2O are 5 ppb and less than 1 ppb, respectively) to solve the above problems. We used a distillation method (boiling point of monosilane, −112°C, disiloxane, −15°C) for SiH_4 purification. For the SiH_4 distillation system and the filling system, we used a stainless steel tube with Cr_2O_3 surface treatment which provides rapid H_2O desorption, little adsorbed moisture volume, and noncatalytic effect. For the cylinder for high-purity SiH_4 gas, a clean stainless steel cylinder (without H_2O adsorption), which resists heat up to 200°C.

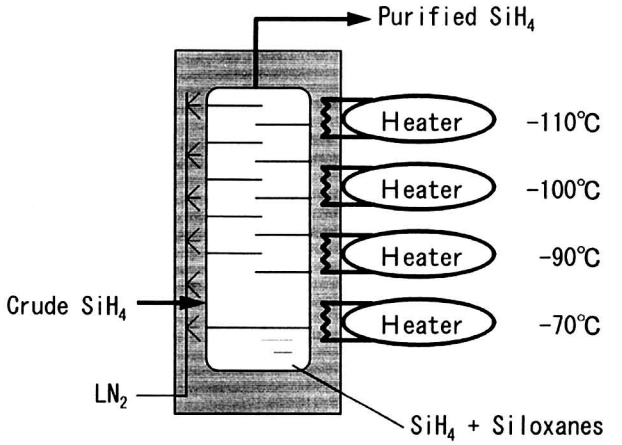

Fig. 16. The distillation system for high purity SiH_4 gas production.

Manuscript received September 22, 1997; revised manuscript received February 6, 1998.

Tohoku University assisted in meeting the publication costs of this article.

REFERENCES

1. T. Ohmi, T. Ichikawa, H. Iwabuchi, and T. Shibata, *J. Appl. Phys.*, **66,** 4756 (1989).
2. T. Ohmi and T. Shibata, in *Proceedings of Semiconductor Manufacturing Technology in the Year 2000*, 1995 Japanese Semiconductor Industry Conference, pp. 00-61, Tokyo (April 1995).
3. T. Ohmi, in *Proceedings of International Symposium on Semiconductor Manufacturing,* ISSM'95, pp. 277-282, Austin, TX (1995).
4. T. Ohmi, S. Miyoshi, Y. Shirai, T. Kojima, and Y. Mizuguchi, *J. Electrochem. Soc.*, **142,** 2362 (1995).
5. Y. Shirai, M. Narazaki, and T. Ohmi, *IEICE Trans. Electron.*, Vol. E79-C, 385 (1996).
6. N. Ikeda, *Compact Ultra Clean Gas Supply System,* Special Program, of Cleanrooms '96 west, The Conference on Advanced Microcontamination Control and Ultrapure Manufacturing, pp. 68-77, Santa Clara, CA (1996).
7. T. Ohmi, Y. Nakagawa, M. Nakamura, A. Ohki, and T. Koyama, *J. Vac. Sci. Technol. A,* **14,** 2505 (1996).
8. Y. Shirai, S. Miyoshi, S. Takahashi, T. Kojima, and T. Ohmi, in *Proceedings of International Conference on AMDDP,* p. 517 (1994).
9. T. Ohmi, M Nakamura, A. Ohki, K. Kawada, and K. Hirao, *J. Electrochem. Soc.*, **139,** 2654 (1992).
10. E. F. Ezell, J. Grob, and P. Clark, in *Microcontamination '94,* Society, pp. 413-424, San Jose, CA (1994).
11. P. R. Solomon, R. M. Carangero, and M. D. Carangelo, *SPIE,* **2366,** 155 (1994); SPIE-Int. Soc. Opt. Eng.
12. M. Reath, J. Brannen, P. Bakeman, and R. Label, *J. IES,* 57 (March-April 1994).
13. J. M. Girard, P. Mauvais, in *Proceedings of ISSM '96,* p. 325, Tokyo (Oct 1996).
14. S. Q. Wu, H. Masusaki, Y. Ishihara, K. Matsumoto, T. Kimishima, J. Morishita, H. Kuze, and N. Takeuch, *Proceedings, of ISSM '96,* p. 321, Tokyo (Oct 1996).
15. M. Nakamura, A. Ohki, T. Kijima, and J. Date, in *Ultra Clean V Group Gas,* The Institute of Electrical Engineers of Japan, MC-96-6, pp. 45-54 (Nov 1996).
16. H. Izumi, Y. Nakagawa, S. Miyoshi, and T. Ohmi, in Extended Abstracts, 1994 International Symposium on Semiconductor Manufacturing, pp. 211-212 (1994).
17. K. Ishikawa, H. Mihira, and T. Ohmi, in *Proceedings of Microcontamination '92,* pp. 98-106, Santa Clara, CA (Oct 1992).
18. Y. Mitsui, T. Irie, S. Iijima, K. Mizokami, K. Hasumi, and K. Kuriyama, in *Proceedings of the 40th Annual Technical Meeting of the IES,* pp. 246-253, Chicago, IL (May 1994).
19. Y. Shirai, S. Miyoshi, T. Kojima, and T. Ohmi, in Extended Abstracts, 1994 International Symposium on

Semiconductor Manufacturing, pp. 217-218, Tokyo (June 1994).
20. Y. Shirai, M. Narazaki, and T. Ohmi, in *Proceedings of IEICE Trans. Electron.*, Vol. E79-C, No. 3, 385-389 (1996).
21. Y. Ikezoe, S. Matsuoka, M. Takebe, and A. Viggiano, *Gas Phase Ion-Molecule Reaction Rate Constants Through 1986*, Maruzen, Tokyo (1987).

A Two-Dimensional Model of Chemical Vapor Infiltration with Radio-Frequency Heating

II. Strategies to Achieve Complete Densification

Vikas Midha and Demetre J. Economou*

Plasma Processing Laboratory, Department of Chemical Engineering, University of Houston, Houston, Texas 77204-4792, USA

ABSTRACT

A two-dimensional finite-element model is used to compare isothermal and radio-frequency-assisted chemical vapor infiltration of long cylindrical carbon preforms. Densification with radio-frequency heating at a constant input power initially occurs radially around the central zone and then axially toward the ends of the preform. This densification pattern results in significant entrapment of porosity at the center of the preform and requires a relatively long time for completion. A novel scheme for improved radio-frequency heating of long cylindrical preforms is proposed which entails insulating the axial ends of the preform, induction heating at a relatively high operating frequency, and linear ramping of input power with time. Simulations show that, under these conditions, radial "inside-out" densification can be achieved uniformly along the entire length of the preform. This scheme results in complete densification of the preform and reduces the overall processing time fivefold when compared to the conventional isothermal process.

Introduction

Chemical vapor infiltration (CVI) has emerged as a leading technique for fabricating fiber-reinforced ceramic composite materials. The conventional CVI process consists of diffusion and chemical reaction of a precursor gas under essentially isobaric and isothermal conditions to deposit solid material within the pores of a fibrous preform. This process, however, is extremely slow and expensive, since low operating temperatures are necessary for uniform densification of the preform. At higher temperatures, the rate of chemical reaction exceeds the rate of mass transfer, leading to premature plugging of pores at the surface of the preform and entrapment of porosity inside the material.

A promising modification to isothermal CVI is to use volumetric heating of the preform. Volumetric heating combined with heat losses from the surface produces an "inverted" temperature gradient in the preform. This temperature profile favors a faster rate of chemical reaction in the interior of the preform as opposed to the surface, thereby minimizing the effect of increased mass-transfer resistance with densification of the preform. CVI with volumetric heating has the potential to achieve rapid and complete densification of preforms. This process has been demonstrated experimentally using microwave,[1] or radio-frequency (RF) induction heating.[2-4]

Existing theoretical studies of CVI with volumetric heating are mostly restricted to one-dimensional (1D) models.[5-9] Moreover, the power distribution due to electromagnetic radiation is treated as constant in both time and space, or constant in time with a distribution corresponding to the initial electrical properties of the preform.[8,9] Recently we reported the development of a 2D finite element model for CVI with RF heating, which self-consistently accounts for the variation in the power distribution as the preform densifies.[10] A mechanism was identified by which more power is deposited in the densified regions of the preform that can potentially lead to thermal runaway. Simulations show that densification of a cylindrical carbon preform proceeds in an "inside-out" manner from the central zone, first in the radial direction and then axially toward the ends. The simulated temperature profiles showed semiquantitative agreement with experimental results reported in the literature.

This study further examines the potential of using RF-assisted CVI (RFCVI) for the densification of cylindrical carbon preforms by the thermal decomposition of methane. First, 2D simulations of isothermal isobaric CVI are presented, since this is the most widely accepted mode of CVI. By studying the influence of operating temperature and pressure, we form a base case for comparison with RFCVI. To be a feasible process, RFCVI must provide a significant improvement in performance compared to isothermal CVI. Next, the densification behavior with RFCVI is compared to that with isothermal CVI. We examine the influence of key operating parameters of RFCVI including total input power, pressure, and the effect of insulation for improving performance. Based on our understanding of the physics of RFCVI, we develop a novel scheme for tailoring RF heating to achieve rapid and complete densification of cylindrical preforms.

Mathematical Model

Figure 1 shows a schematic of the CVI apparatus modeled in this study. A cylindrical 3D carbon preform is placed coaxially at the center of the reactor. A helical RF induction coil is used to heat the preform to the desired operating temperatures. The entire assembly is enclosed in a metallic chamber to contain radiation. Details of the mathematical model formulation and the finite-element solution were presented earlier in Ref. 10. Therefore, only the salient features of the model are repeated here and modifications in the mathematical formulation are emphasized. For convenience, the mathematical model may be divided into two modules: the electromagnetic (EM) module and the CVI module. The governing equations of the two modules are summarized in Table I.

The EM module solves Maxwell's equations for the electromagnetic fields and the power distribution in the preform due to the induction coil. Since the electrical properties of the material evolve with porosity over time periods of several hours, the electromagnetic oscillations are assumed to be time-harmonic in nature. This enables the solution of the electric field in the frequency-domain as opposed to the time-domain. Azimuthal symmetry is im-

* Electrochemical Society Active Member.